4-2018

Design optimization of polymer heat exchanger for automated household-scale solar water pasteurizer

David C. Denkenberger
Tennessee State University

Joshua M. Pearce
Michigan Technological University

designs

MDPI

Article

Design Optimization of Polymer Heat Exchanger for Automated Household-Scale Solar Water Pasteurizer

David C. Denkenberger [1,2] and Joshua M. Pearce [3,4,*]

1 Tennessee State University, Civil and Architectural Engineering, 3500 John A Merritt Boulevard, Nashville, TN 37209, USA; ddenkenb@tnstate.edu
2 Alliance to Feed the Earth in Disasters (ALLFED), Nashville, TN 37209, USA
3 Department of Electronics and Nanoengineering, School of Electrical Engineering, Aalto University, Espoo 02150, Finland
4 Department of Materials Science & Engineering and Department of Electrical & Computer Engineering, Michigan Technological University, Houghton, MI 49931, USA
* Correspondence: pearce@mtu.edu; Tel.: +1-906-487-1466

Received: 23 March 2018; Accepted: 18 April 2018; Published: 21 April 2018

Abstract: A promising approach to reducing the >870,000 deaths/year globally from unsafe water is flow-through solar water pasteurization systems (SWPs). Unfortunately, demonstrated systems have high capital costs, which limits access for the poor. The most expensive component of such systems is the heat exchanger (HX). Thus, this study focuses on cost optimization of HX designs for flow-through SWPs using high-effectiveness polymer microchannel HXs. The theoretical foundation for the cost optimization of a polymer microchannel HX is provided, and outputs are plotted in order to provide guidelines for designers to perform HX optimizations. These plots are used in two case studies: (1) substitution of a coiled copper HX with polymer microchannel HX, and (2) design of a polymer microchannel HX for a 3-D printed collector that can fit in an arbitrary build volume. The results show that substitution of the polymer expanded HX reduced the overall expenditure for the system by a factor 50, which aids in making the system more economical. For the second case study, the results show how future system designers can optimize an HX for an arbitrary SWP geometry. The approach of distributed manufacturing using laser welding appears promising for HX for SWP.

Keywords: distributed manufacturing; heat exchanger; laser welding; microchannel; open hardware; optimization; solar energy; solar thermal; solar water pasteurization; water pasteurization

1. Introduction

Throughout the world, an estimated 871,000 deaths were due to unsafe water in 2012 [1]. Deaths from unsafe water include those caused by diarrhea, intestinal nematode infections and protein-energy malnutrition attributable to lack of access to water [1]. They also include deaths from lack of access to appropriate water sanitation and hygiene (WASH) services [1]. These deaths primarily occur in low-income communities and strike young children under 5 years old the hardest [2,3]. The global coverage of safely-managed drinking-water services remains unacceptably low with only 68% coverage in urban areas and 20% in rural areas [4,5]. Although this problem would be easily solved with a more even distribution of wealth [6], current political circumstances continue to provide an urgent need for low-cost water disinfection methods, which can be mass-deployed for the poor in the developing world. There have been various methods attempted to provide drinking water in rural areas of undeveloped nations using solar technologies, including: (i) solar desalination; (ii) solar detoxification; and (iii) solar disinfection [7,8]. These methods include the use of basic solar

stills [9,10], solar stills with improved output from compound parabolic reflectors [11], phase change material [12], a hemispherical solar still [13], efficient heat exchange mechanisms [14] and an inclined wick solar still [15], and progressively more sophisticated variations of the solar water disinfection (SODIS) method [16], using common chemicals to decrease turbidity to enable SODIS to work [17] and photocatalysts [18]. SODIS is low-cost, simple, and is available for large geographic regions (e.g., from Haiti [19] to South Sudan [20]), but becomes less effective in high-turbidity water, which can be challenging in some communities [16]. Previous simulations [21,22] have shown that although solar stills have an advantage with chemically contaminated water and salt water, solar water pasteurization (SWP) is more efficient and less costly for water disinfection. Many types of SWP systems have been developed [23,24], including simple systems with reflectors [25,26], systems based on density difference flow principles [27], parabolic trough concentrator systems [28,29], and continuous flow systems, which are the focus of this study [30–33]. Continuous flow systems have been shown to be effective at sterilizing water [34], and a kiosk system can be constructed for US$2000 [35]. This is too much of an investment for individual families and even many communities. Previous numerical simulation of SWPs found enormous increases in drinkable water output from contaminated sources by incorporating optimized compound parabolic concentrating (CPC) reflectors into the system (depending on the climate, CPCs increase output in pasteurizers by 1000–4000%) [22]. The increase in outputs are so phenomenal they could be applied to provide clean safe drinking water in the worst case scenarios: long-term isolated areas with no electricity or other sources of energy, no transportation capabilities for bringing in clean water, and no specialized equipment or materials.

However, to make this possible for many communities and households, the costs of such systems must be reduced. To enable such high-performance solar water pasteurization systems to be deployed in developing communities at low costs, in this study an approach known as open-source appropriate technology (OSAT) [36] is applied. It uses open-design-based strategies [37,38] to harness recent advances in distributed manufacturing [39] with digital designs to reduce the costs of a system. Solar-powered distributed manufacturing has already been demonstrated [40,41], which makes even remote or off-grid manufacturing feasible. In general, the most expensive and most critical system component for highly efficient flow-through SWP systems is the heat exchanger (HX). Thus, this study will focus on the cost optimization of HX designs for SWP systems in order to reduce the costs of the entire systems to be economically viable in the developing world. This study will be limited to the methods of fabrication that use open-source distributed manufacturing.

This study will provide for the first time a method of cost optimization of HX designs for SWP systems fabricated using fully open-source distributed manufacturing. Specifically, this paper first provides the background on flow-through SWP systems and polymer microchannel HXs, their manufacture, and how to achieve high effectiveness. Next, the theoretical foundation for the cost optimization of a polymer microchannel HX is provided and outputs are plotted in order to provide guidelines for designers to perform optimizations for such HXs. These results are used in two case studies: (1) substitution of a coiled copper HX with polymer microchannel HX; and (2) design of a polymer microchannel HX for a 3-D printed collector that can fit in an arbitrary build volume. The results are presented. The challenges and economics of polymer HXs used for flow-through SWP systems are discussed and conclusions are drawn.

2. Background

A nomenclature Table is provided in Appendix A, which includes units and explanations of all symbols and subscripts.

2.1. Flow-Through Solar Water Pasteurizer

Boiling water is not necessary to make biologically contaminated water safe to drink, as all microbes that cause disease in humans are unable to survive at temperatures exceeding 65 °C, which passive solar thermal devices can easily produce [42]. A flow-through SWP contains

a thermostatic valve that opens when the water reaches a threshold temperature (indicating pasteurization), and the outgoing hot water warms the incoming cool water in a heat exchanger (Figure 1). The flow is caused by the dirty water reservoir being at a higher elevation than the clean water reservoir. The addition of the heat exchanger and the valve increase the output by a factor of eight or more [42]. With a 70 °C valve temperature and an 87.5% effective HX, with the entering water temperature (ambient) of 30 °C, the water entering the solar collector will be at 65 °C, which is already at the pasteurization temperature. This should guarantee that the water is pasteurized despite some non-uniform illumination and temperature gradients resulting from the heat conducting down through the tubing. It is clear that a low-cost HX design is critical for this application.

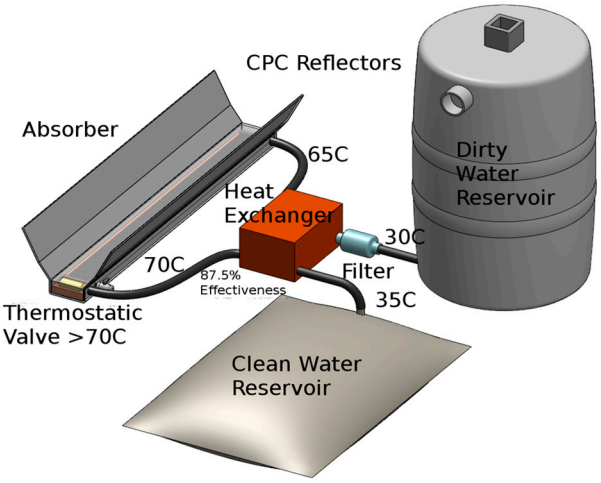

Figure 1. Labeled schematic of the primary components of a flow-through solar water pasteurizer.

2.2. Microchannel Heat Exchangers

Heat exchangers transfer heat from one fluid to another (in this case from the hot pasteurized water to the cool dirty water). Traditionally, they are made from metal, because of the high thermal conductivity of metals; however, polymers can also be used to make effective HXs [43]. The performance of a HX for SWPs is characterized by its effectiveness, η, defined as the realized heat transfer rate as a fraction of the maximum heat transfer rate:

$$\eta = \frac{\dot{q}}{\dot{q}_{max}} \tag{1}$$

where the realized heat transfer rate is:

$$\dot{q} = C(T_{hi} - T_{ho}) = C(T_{co} - T_{ci}) \tag{2}$$

where the temperature of the hot pasteurized water entering the HX is T_{hi}, the temperature of the hot pasteurized water exiting the HX is T_{ho}, the temperature of the contaminated cold water entering the HX is T_{ci}, and the temperature of the contaminated cold water exiting the HX is T_{co} [6]. SWPs have balanced flow, so the heat capacity rate is:

$$C = \dot{m}C_p \tag{3}$$

where the mass flow rate $\dot{m}$ and the specific heat is C_p. The maximum heat transfer rate is:

$$\dot{q}_{max} = C(T_{hi} - T_{ci}) \tag{4}$$

For a counter-flow HX with balanced flow,

$$\eta = \frac{NTU}{NTU + 1} \tag{5}$$

where NTU is "number of transfer units",

$$NTU = \frac{hA}{C} \tag{6}$$

where A is the heat transfer area and h is the heat transfer coefficient.

Microchannel HXs (defined as those with a hydraulic diameter <1 mm) are currently used, and they have reduced material cost, weight, and volume, but the standard mass-manufacturing techniques that include etching, LIGA (lithography, electroplating and molding), micromachining, and stereolithography are expensive [44]. In addition, laser welding can be used to fabricate microchannel HXs [45]. Using reverse conduction laser welding, it is even possible to weld transparent polymers [46]. For the welding of polymers, the temperature must be above the melting temperature, but below the decomposition temperature. This temperature difference, or viable range, influences how easy it is to laser-weld a polymer [47]. Some suitable polymers for this are low-density polyethylene (LDPE), linear low-density polyethylene (LLDPE), high-density polyethylene (HDPE), polypropylene (PP), and polystyrene (PS). An open-source laser polymer welding system was developed [48] and refined [49] to radically reduce manufacturing costs of polymer HXs. Recent experiments have shown that polymer-based wall thermal resistance is no longer the limiting factor for such HXs [50] and the designs have been applied to water-air HXs [50] and air-air HXs [51]. In this study, water-water HX designs for microchannel HXs will be evaluated in detail.

2.3. Approaches to Achieving High Effectiveness with Polymer Microchannel HXs

Most current HXs experience turbulent flow, which produces a high heat transfer coefficient; while for microchannel HX at smaller channel hydraulic diameters, the flow becomes laminar, which reduces the heat transfer coefficient. However, at even smaller diameters, the distance that the heat has to conduct through the fluid becomes short, so heat transfer coefficient increases, even exceeding the turbulent heat transfer coefficient for very small channels. Furthermore, with laminar flow, when velocity is decreased, heat transfer coefficient is maintained (constant Nusselt number (Nu), which is the ratio of the thermal resistance in the fluid without convection to the thermal resistance with convection). Since the pumping loss decreases with lower velocity, the pump power can be made very low by having many parallel channels.

The low thermal conductivity of polymers would appear to be a barrier to achieving high effectiveness. However, this limitation can be overcome with proper wall thickness and channel size. The following discussion is based on [45]. Consider a polymer microchannel HX with adjacent same-sized tubes, which can be achieved with square passages or hexagonal passages. For non-finned surfaces, no fouling, thin walls, and equal convective heat transfer coefficients on both sides, the overall heat transfer coefficient is:

$$U = \frac{1}{\frac{2}{h} + \frac{t_w}{k_w}} \tag{7}$$

where h is the heat transfer coefficient in each of the fluids (cold contaminated water and hot pasteurized water), t_w is the thickness of the wall, and k_w is the thermal conductivity of the wall. If the effect of wall thickness is analyzed for a material with k_w = 0.2 W/(mK), typical of polymers, the following conclusions can be drawn for various flow configurations:

- 1 mm polymer wall thickness has little effect when h ~100 W/(m^{2}K), which turbulent gas flow or with laminar gas flow in 1 mm diameter channels can achieve.

- 0.1 mm polymer wall thickness has little effect when h ~1000 W/(m^{2}K), which laminar gas flow in 0.1 mm diameter tubes or with turbulent liquid flow or laminar liquid flow in 1 mm channels can achieve.
- 0.01 mm polymer wall thickness has little effect when h ~10,000 W/(m^{2}K), which laminar liquid flow in 0.1 mm diameter channels can achieve.

Other factors also reduce the drawback of low polymer thermal conductivity. Surface fouling, on both metal and polymer HXs, increases the thermal resistance and makes the lower-conductivity materials relatively less consequential. Finally, the low thermal conductivity of a polymer can actually be an advantage for high-effectiveness HXs, because it reduces axial conduction.

A significant benefit of polymer HXs compared to metal HXs is low material price. Multiplying the thickness of the material t and the price of the material P_V yields the price per area. Dividing this by the overall heat transfer coefficient yields the material price per heat transfer ability:

$$P_{HT} = P_V \cdot \frac{t}{U} \tag{8}$$

For a constant ratio between wall thickness and channel diameter (in this case 0.1), both the overall thermal resistance and material price per heat transfer area are proportional to the diameter. The product of these, P_{HT}, varies with the square of the diameter. Therefore, a small diameter is highly beneficial. Preliminary analysis thus suggests that microchannel polymer HXs can be designed with small channel diameter, thin walls, low velocity, short flow lengths, and large face areas to produce high effectiveness and low initial costs.

3. Materials and Methods

In order to optimize the design of the HX for solar thermal water pasteurization, this analysis will take the approach of minimizing the sum of the HX and life cycle "fuel" expenditures. In this application, the HX is non-essential, as the process will simply require more solar energy (large collector) if no HX is used. Ineffectiveness is one minus effectiveness. The assumptions include the standard ones for heat exchangers: (1) no axial or longitudinal conduction (along the flow); (2) no heat loss to the environment; (3) no flow maldistribution (all channels receive the same amount of flow); (4) constant fluid properties; and (5) a constant heat transfer coefficient. The equations apply to both laminar and turbulent flow. The efficiency equals effectiveness, so the expenditure on solar is:

$$E_{fuel,n-e} = k_3(1 - \eta) \tag{9}$$

where

$$k_3 = \frac{\dot{m} C_p \Delta T_f P_{solar} H}{278,000 r} \tag{10}$$

where $\dot{m}$ is the mass flow rate in kg/s, C_p is the specific heat in J/(kgK), ΔT_f is the temperature change of the water in K (either $T_{h,i} - T_{h,o}$ or $T_{c,o} - T_{c,i}$), P_{solar} is the price of solar in \$/GJ, H is the number of hours per year, r is the interest rate ($1/r$ is roughly the time horizon), and 278,000 is the constant to make U.S. dollars the units of k_3 (one billion conversion between GJ and J divided by 3600 s per hour yields 278,000). The solar expenditure is proportional to the ineffectiveness because the solar provides the heat that is not reclaimed. k_3 can be thought of as the "load". In the pasteurizer case, the load is the energy required to heat the water and the HX reduces the fraction of this energy that has to be provided by solar.

The simple model assumes that the material, manufacturing, and life cycle head loss expenditures are proportional to A for a given channel diameter and wall thickness:

$$E_{HX} = k_1 A \tag{11}$$

where

$$k_1 = P_v t \tag{12}$$

where P_v is the equivalent price of the wall material in \$/m^3, t is the wall thickness in m, so the units of k_1 are U.S. dollars/m^2.

Counter-flow is appropriate when the two fluids have similar heat capacity rates (the product of density, heat capacity, temperature change, and flow rate) as is the case for the water pasteurizer. Therefore,

$$\eta = \frac{1 - \exp\left(-NTU(1-C)\right)}{1 - Cexp(-NTU(1-C))} \tag{13}$$

where C is the heat capacity rate ratio, $C_{\min}/C_{\max}$, and

$$NTU = \frac{A}{k_2} \tag{14}$$

where A is the heat transfer area in m^2 and

$$k_2 = \frac{\dot{m}C_p}{U} \tag{15}$$

where U is the overall heat transfer coefficient in W/(m^{2}K). For the SWP non-essential case,

$$E_{fuel,n-e} = \frac{k_3(1-C)\exp\left(\frac{-A(1-C)}{k_2}\right)}{1 - C\exp\left(\frac{-A(1-C)}{k_2}\right)} \tag{16}$$

The total expenditure is the sum of the HX expenditure and the solar expenditure:

$$E_{t,n-e} = E_{HX} + E_{fuel,n-e} = k_1 A + \frac{k_3(1-C)\exp\left(\frac{-A(1-C)}{k_2}\right)}{1 - C\exp\left(\frac{-A(1-C)}{k_2}\right)} \tag{17}$$

Setting the derivative with respect to A of $E_{t,n\text{-}e}$ equal to zero, and solving, provides:

$$A_{opt,n-e} = \frac{k_2 LN\left(\frac{\Theta_{n-e}}{C^2 k_1 k_2}\right)}{C-1},\ C \neq 1,\ C \neq 0 \tag{18}$$

where

$$\begin{aligned}\Theta_{n-e} = 0.5k_3 - Ck_3 + Ck_1k_2 + 0.5C\left(k_3(k_3C^2 - 2k_3C + k_3 + 4Ck_1k_2)\right)^{0.5} + 0.5C^2k_3 \\ -0.5\left(k_3(k_3C^2 - 2k_3C + k_3 + 4Ck_1k_2)\right)^{0.5}\end{aligned} \tag{19}$$

For the special case of C = 1, the starting equations are the same or simpler in the case of effectiveness; Equation (5). The result of the derivation for the SWP non-essential case is:

$$A_{opt,n-e} = k_2\left(\left(\frac{k_3}{k_1k_2}\right)^{0.5} - 1\right) \tag{20}$$

For C = 0 non-essential (perfectly unbalanced flow, not the SWP), again there is a simpler equation for effectiveness:

$$\eta = 1 - e^{-NTU} \tag{21}$$

The result of the derivation for this case is:

$$A_{opt,n-e} = k_2 LN\left(\frac{k_3}{k_1k_2}\right) \tag{22}$$

In the next section, a subset of these equations is plotted and used to calculate real-world examples.

4. Results

4.1. Simulation Results

Equations (9) and (10) are used to make Figure 2.

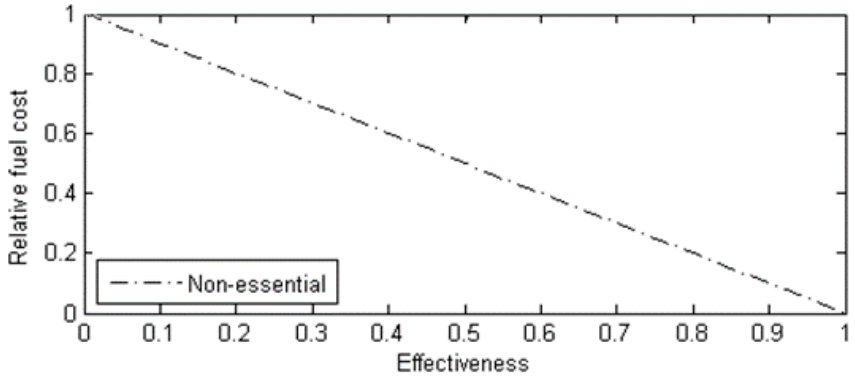

Figure 2. Relative solar expenditure for non-essential cases like the heat exchanger for solar water pasteurization as a function of effectiveness from 0 to 1.

The results are plotted (Figure 3) as a function of the non-dimensional expenditure:

$$E_{n-d} = \frac{k_1 k_2}{k_3} = \frac{P_{NTU}}{k_3} \tag{23}$$

where P_{NTU} is the price per *NTU*. For $E_{n\text{-}d}$ = 1, the price of an *NTU* is equal to the "load". For non-essential SWP, the optimum HX *NTU* = 0, so ineffectiveness = 1. For low non-dimensional expenditure ($E_{n\text{-}d}$), for *C* = 1 (balanced flow), slope = 0.5, and for *C* = 0 (perfectly unbalanced flow), slope = 1.

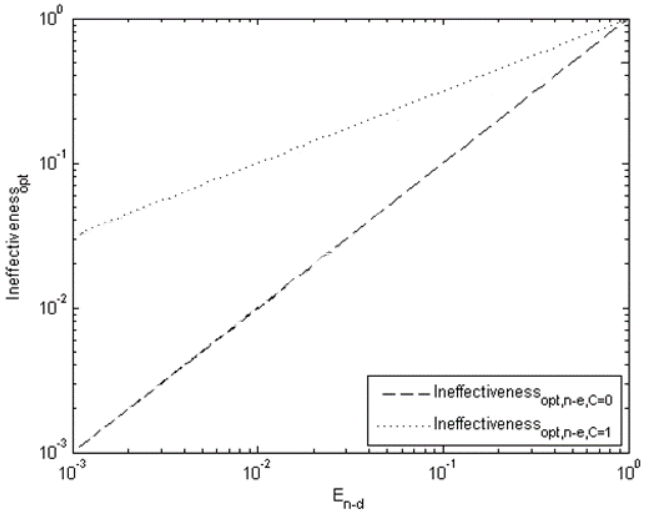

Figure 3. Optimum ineffectiveness as a function of $E_{n\text{-}d}$ the non-dimensional expenditure.

Non-dimensional expenditure was varied by varying the equivalent material price. This is equivalent to varying the other parameters that affect the price per heat transfer ability, including thickness and all the factors that go into the overall heat transfer coefficient: channel diameter, Nusselt number, and thermal conductivities. The non-essential solar expenditures display the same behavior as the ineffectiveness because they are proportional (see Figure 4). For low non-dimensional expenditure

and C = 1 (balanced flow), solar and HX expenditures are equated, similar to the case of building insulation optimization [52]. For high non-dimensional expenditure, HX expenditures tend to zero, because the HX area tends to zero.

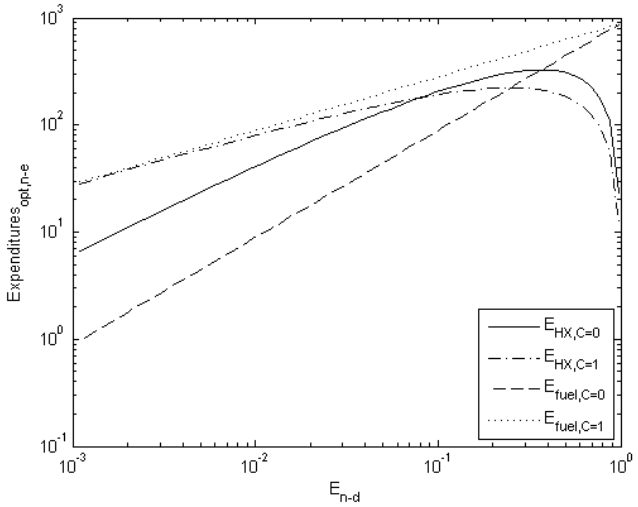

Figure 4. Non-essential solar expenditures and HX expenditures as a function of non-dimensional expenditure.

For C = 1 (balanced flow), slope = 0.5 for HX and solar expenditures. For C = 0 (perfectly unbalanced flow), slope = 1 for solar expenditures. However, if there were an order of magnitude reduction in non-dimensional expenditure, for there to be an order of magnitude reduction in the HX expenditure, the HX would have to stay the same size, which is not consistent with the solar expenditure falling. To have an order of magnitude reduction in ineffectiveness, 2.3 *NTU* must be added. At high non-dimensional expenditure, this represents a large fraction increase in the area, so HX expenditure does not fall fast. However, at low non-dimensional expenditure, 2.3 *NTU* represents a small fraction increase in the area, so HX expenditure falls fast, approaching an order of magnitude with an order of magnitude non-dimensional expenditure reduction, or a slope of unity.

The optimization can be used not just for calculating the advantages of the expanded HX, but also for parameter changes in general heat exchangers. For instance, if mass flow rate quadruples, the inverse of the area required for one NTU (k_2) and load (k_3) also quadruple, so the non-dimensional expenditure stays constant. Therefore, the optimal ineffectiveness remains the same for a larger HX and system (this analysis ignores cost economies of scale). However, the HX and fuel expenditures quadruple (the curves in Figure 4 shift upward by a factor of four). Some parameters only affect load (k_3), such as fluid temperature change, price of fuel, hours per year of operation, and interest rate. Quadrupling the first three or reducing interest rate by a factor of four would each quadruple k_3. For a low non-dimensional expenditure, the optimum ineffectiveness is halved for C = 1 (balanced flow), and quartered for C = 0 (perfectly unbalanced flow) for this scenario. The resulting shift in the HX and fuel expenditure curves produces for C = 1 a doubling in HX and fuel expenditures for low non-dimensional expenditure. For C = 0 and low non-dimensional expenditure, fuel expenditure remains constant, and HX expenditure increases slightly.

Figures 3 and 4 apply for laminar flow or turbulent flow. For turbulent flow, the overall heat transfer coefficient varies with the fluid velocity. In this case, the price per heat transfer ability in average conditions should be used. The effect of channel diameter scaling on the overall heat transfer coefficient is complicated for turbulent flow, so general conclusions cannot be drawn. However, for laminar flow where the overall heat transfer coefficient is independent of fluid velocity, further conclusions can be drawn. Combining the slope = 2 behavior of price per heat transfer ability with the channel diameter and the slope = 0.5 behavior of ineffectiveness with price per heat transfer ability for

the optimal non-essential HX with $C = 1$ (Figure 4), the optimal ineffectiveness falls with the channel diameter for laminar flow. If the 1 mm channel diameter has similar heat transfer coefficient to a typical turbulent case but a factor of 30 reduction in the price per area (and thus non-dimensional expenditure), and if the turbulent case has $\eta = 60\%$, the optimal η ~93%. Furthermore, going to a 0.3 mm tube diameter, the optimal η ~98%.

For non-essential $C = 0$ (perfectly unbalanced flow), the slope = 1 in Figure 3, so combining the slope = 2 behavior of price per heat transfer ability with channel diameter, the optimal ineffectiveness falls with channel diameter squared. Therefore, if the 1 mm channel diameter has similar h to a typical turbulent case, but a factor of 30 reduction in the price per area (and thus non-dimensional expenditure), and if the turbulent case has $\eta = 60\%$, the optimal η ~98.7%. Furthermore, going to a 0.3 mm tube diameter, the optimal η ~99.8%. This is not for a cost-independent application of cryogenics in space, but an everyday application. In reality, other factors, such as heat leak (heat gain or loss to the surroundings), axial conduction, and flow maldistribution (flow in channels not being equal), start to dominate. However, large HXs have a small percentage of heat leak and axial conduction. Furthermore, multiple serial stages of cross-flow HXs can be used to approximate counter-flow effectiveness [53]. Similarly, though flow maldistribution limits the effectiveness of a single stage, multiple stages can be used to mitigate the effect of maldistribution, so analysis indicates that low-cost HXs should have high effectiveness.

4.2. Case Study 1: Substitution of Metal HX with Polymer HX in Solar Water Pasteurizer

An example SWP has a 6 m^2 \$300 flat plate solar collector, a HX that is \$200 and has $\eta = 66\%$ [54]. The HX is made of coiled copper tubing arranged in a counter-flow pattern and dipped in solder to increase the heat transfer between the hot and cold tubes. At zero effectiveness, the collector would cost \$900, so this is load (k_3). The system pasteurizes 1000 L/day, so if there are four full sun hours per day, and if the water is flowing the entire time the sun is shining, this would be four hours per day, or H ~1400 h. The mass flow rate would be 0.07 kg/s. This system has a valve opening temperature of 80 °C. With an ambient temperature of 25 °C, the total temperature difference for the heat exchanger $\Delta T_t = T_{h,i} - T_{c,i} = 55$ °C. With $\eta = 66\%$, the entering cold water is warmed to 61 °C, so the internal HX $\Delta T_i = 19$ °C (logarithmic mean temperature difference, but for balanced flow, it is simply $T_{h,i} - T_{c,o} = T_{h,o} - T_{c,i}$. The heat flow is the mass flow rate times specific heat times temperature change of one of the fluids in the HX (36 °C), or 11,000 W (Equations (2) and (3)). To transfer 11,000 W at 19 °C temperature difference requires $UA = 550$ W/K. Therefore, P_{HT} = \$200/(550 W/K) = \$0.36/(W/K). This covers the material and manufacturing costs, and the pumping costs are small because it is gravity driven (the water is lifted by hand to the higher reservoir or provided by rain water harvesting and gravity from a roof or other collection surface [55,56]. It should be noted that harvested rainwater is often microbiologically contaminated and needs pasteurization [56,57]. Since $\eta = 66\%$, by Equation (5), $NTU = 2$. Since the HX costs \$200, price per $NTU = P_{NTU}$ = \$100. Then, by Equation (22), the corresponding $E_{n\text{-}d} = 0.11$; so from Figure 3, the optimal ineffectiveness for $C = 1$ (balanced flow) is 33%, which agrees very well with the value chosen in practice after trial and error for the SWP of 34%.

If the current copper HX were replaced with a HX with the parameters of the prototype in [45] with 28 μm thick LDPE but mass produced (close to material price), with \$2000/m^3 and $U = 500$ W/(m^2K), by Equation (8), P_{HT} = \$0.00011/(W/K). For the experiments in this previous work, the Reynolds number of the channels was 0.14–10, which is highly laminar. These experiments validated the model. This corresponds to a factor of 3000 reduction in the price per heat transfer ability and thus non-dimensional expenditure. Unfortunately, this is beyond the bounds of Figure 3. However, a slope of 0.5 indicates that the 3000x advantage is equally apportioned to reducing the ineffectiveness and reducing the total expenditure on the HX, both being reduced by $3000^{0.5} = 55$x. Therefore, extrapolating yields an optimal ineffectiveness of 0.6%, and the collector and HX expenditure would be ~\$5 each.

Therefore, the expanded HX reduced the overall expenditure for the HX/collector system by a factor of ~50, which aids in making the system more economical.

Tying this back to the original four equations, the effectiveness is 99.4%. Inlet HX temperatures are 80 °C for hot flow and 25 °C for cold flow. Outlet HX temperatures are 25.3 °C for (initially) hot flow and 79.7 °C for (initially) cold flow. If the flow rate of 1000 L/day is spread out over the 4 full sun hours, this would be 0.07 kg/s mass flow rate. The specific heat of water is 4180 J/(kgK). Therefore, the heat capacity rate is 300 W/K. Thus, the maximum heat transfer rate is 15,960 W and the actual heat transfer rate is 15,880 W (non-significant figures are shown for clarity). Neglecting heat losses in the insulated piping, this means the solar energy requirement is the difference between maximum and actual heat transfer of 80 W. With a collector efficiency of 70% when the sun is shining, this would correspond to 110 W solar input. This corresponds well to a collector area of 0.11 m^2, as it is about 1000 W/m^2 incident solar energy during the full sun hours.

4.3. Case Study 2: Design for 3-D Printed Collector of Arbitrary Size

There is a growing interest in the use of 3-D printers for sustainable development [58,59] and disaster relief [60,61]. By using distributed manufacturing of goods, the only inputs are energy and raw materials, which typically use less storage and transport space, are more durable and require significantly less packaging than the actual goods needed in a disaster response [62,63]. Oxfam [64] and the American Red Cross [65,66] are already considering the use of 3-D printing for their work. Currently, 3-D printing cannot completely replace traditional logistics, but by integrating 3-D printing into a humanitarian response, the efficiency of the larger relief effort can be increased [67]. 3-D printers meant to be used in these applications have already been designed [68] and re:3D, an open-source 3-D printing company, has a well-developed interest in seeing their gigabit 3-D printer used for such applications [69].

This case study will consider the use of a Gigabot (3+) (manufactured by re:3D) to fabricate a collector and CPC in one piece. The Gigabot 3+ has a build area of 590 × 600 × 600 mm, which would provide more than enough space to fabricate a collector for the household scale SWP (24 L/day). With the effectiveness of the HX above, and taking into account cloudy days, the collector would only have to be approximately 0.01 m^2. This is with no reflectors, but reflectors could allow the collector to be even smaller. The absorber could be fabricated in the same way as the HX with laser welding and expansion. The pattern could be similar to the "straight" flow configuration layers in the expanded HX [45]. However, the comparative advantage of expansion is not as large as in HXs, so it may be most economical to additively manufacture the absorber with the 3-D printer itself. To minimize the absorber cost, small-diameter parallel channels should be used. Black polymer would absorb the sunlight and protect the polymer from UV. There are several commercially available 3-D printing filaments that are UV resistant, such as ultem (a polyether imide (PEI)) and ASA (acrylonitrile styrene acrylate). Ultem prints at 360–390 °C, and thus requires a high-temperature extruder, but has good thermal properties, dimensional stability, inherent flame retardancy, and good chemical resistance [70]. ASA prints at 250 °C and has good outdoor and UV stability [71]. Insulation can be placed or sprayed around the sides and back to reduce heat loss. A clear cover should be used above the absorber (i.e., polycarbonate).

5. Discussion

5.1. Challenges of Polymer HXs

There are two challenges that must be addressed with microchannel HXs: fouling and erosion. There are a variety of solutions to chemical fouling, including dilution, prevention of deposition on the walls by magnetic means, and scale removal by physical or chemical means [72]. Fouling can also be due to physical means, for instance, particle deposition. In standard HX design, it is recommended that the particles be less than one third the channel size to avoid clogging [73]. Since fouling with

polymers is less of a problem than with metals because the polymers are hydrophobic and expand more with temperature changes, shedding fouling coatings [43], the particles could be at least as large as one third the channel size for polymers.

The wall of the HX can also be physically eroded. The erosion rate of polymer pipes is generally less than that of metal pipes, and the wear decreases with particle size and velocity, with a higher exponent than unity [74]. Assuming that the wall thickness scales with the channel dimension, the particle size will scale with the wall thickness to avoid clogging, and since the erosion rate falls faster than the particle size, this means that percent erosion rate of the wall thickness would be smaller. Therefore, wall erosion is not likely to be a serious problem for microchannel HXs, especially polymer ones.

5.2. Economics

The competitive advantages of household-scale solar water heat pasteurizers include local (even family) control, availability and ease of use. However, CPC SWPs are not likely to become widespread unless they achieve superior economic performance to water trucking, electric water purifiers and conventional water treatment. Water trucking costs vary widely by location, demand, and cost of inputs. In cities, 220 V electricity-driven 3-step branded water purifiers are sold for around US$150. Large-scale water treatment costs ~0.03 cents/L (and then with distribution: 0.1 cents/L). Electric purifiers and large-scale treatment are generally only viable in cities.

A typical rural developing country household size is around six (~7 in sub-Saharan Africa and ~5 for India [75]). With the average adult needing 4 L/day (water used in cooking is pasteurized, and soap cleans the water used for washing, but there is also rinsing vegetables), the SWP needs to produce 24 L/day minimum average (over the storage time of the clean water reservoir). One recommendation was $1 per person per year in 2004 [76], so with inflation and a lifetime of 5 years, the device must have a cost of $40 or less. Typically, the HX and collector are the most expensive components. Scaling down from the SWP above with the expanded microchannel HX would mean the sum of HX and collector would cost <$1. In reality, there would be economies of scale, and the cost would not be that low, but this demonstrates the cost feasibility. Competing technologies, such as UV treatment, could also be done on the village scale, but would require the consumable UV lamps, more technically challenging maintenance of the battery/photovoltaic system, and extensive filtration to ensure water clarity.

5.3. Future Work

Due to the improved performance of distributed digital manufacturing tools, a flow-through solar water pasteurization system can now be constructed using a combination of laser-welded sheets additive manufacturing (AM), fused filament fabrication or fused pellet-shard RepRap-class 3-D printing, and the use of bulk commodity purchased parts available through much of the world, as detailed in Figure 5.

The same laser-welding AM (l in Figure 5) approach could be used for the clean water reservoir and the absorber as well as the HX, which would be expected to have a similar cost reductions as seen in the HX. To reduce the costs of the household-scale solar water heat pasteurizers, digital additive manufacturing with fused filament RepRap-class 3-D printers can be applied to all of the components labeled r in Figure 5, including the fittings, absorber and CPC base. The filter holder, as well as all of the fittings, could also be 3-D printed on a small system [77]. Finally, the tubing, pipe insulation, thermostatic valve, and cover sheet can be purchased from local retailers, as they are all relatively low-cost components. The tubing and insulation are already being mass-manufactured, and are available. The thermostatic valve, although it is mass manufactured for automobiles, could possibly be redesigned to be digitally manufactured, as well. The final component, the dirty water reservoir, may already exist in most locations needing a SWP, and can be purchased or locally manufactured following [55]. Using this approach would be expected to reduce the costs to approximately the

cost of raw materials, in which case a <$40 system is economically feasible. For example, as noted in case study 2, the structure for the reflectors and the absorber can be 3-D printed. To minimize the costs, recycled plastic could also be used. There have been substantial recent developments in converting waste plastic/recycled plastic in 3-D printing filament with a recyclebot (waste plastic 3-D printer filament extruder [78]) and then use it for 3-D printing. Thermopolymer processes already developed include polylactic acid (PLA) [79–82], high-density polyethylene (HDPE) [78,83], acrylonitrile butadiene styrene (ABS) [84–86], as well as waste wood composites [87] and carbon fiber reinforced composites [88]. Future work is needed to design and optimize each of these components, as well as an overall cost optimization of the system. Simultaneously, optimal settings for the digital manufacturing of the open-source designs can be developed and shared, along with the designs on OSAT centers like Appropedia.org [89], to leverage lateral distribution methods.

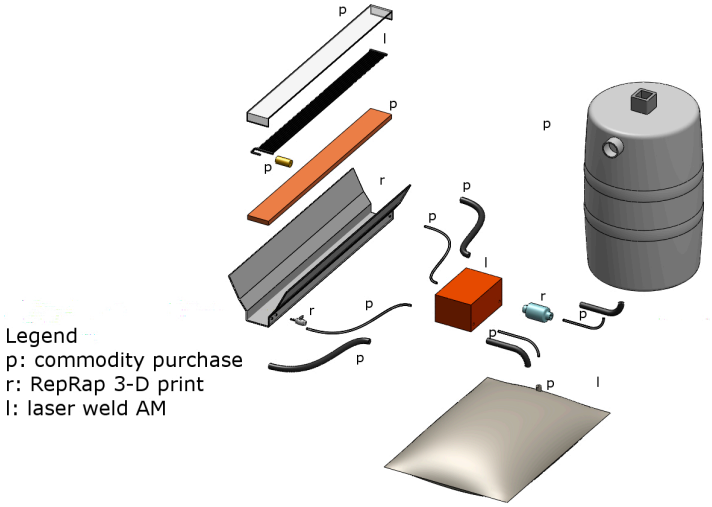

Figure 5. Distributed manufacturing method or purchase of flow-through SWP system.

6. Conclusions

Modeling indicates that high effectiveness can be achieved with polymer HXs for SWP. The new expanded microchannel HX has low materials cost and can be manufactured digitally with low-cost open-source additive manufacturing tools. This optimization is valid for laminar and turbulent flow and applications where the life cycle expenditure for the system to which the HX is connected scales with ineffectiveness (non-essential as in the case of SWP. The optimum effectiveness is higher in cases of higher fuel price, greater hours of operation, greater fluid temperature change, and a longer time horizon, but the HX costs more. However, if the manufacturing and material costs of HXs can be reduced, the optimal effectiveness is higher and the total HX expenditure is lower. Applying these results to the case studies shows that (1) substitution of the polymer-expanded HX reduced the overall expenditure for the system using a metal HX by a factor 50; and (2) future system designers can optimize an HX for an arbitrary SWP geometry. Furthermore, when the HX optimization is applied to SWP, the systems could be manufactured using low-cost open-source AM tools. Thus, it has the potential to be scaled laterally where companies and communities can use the open hardware designs to digitally manufacture their own SWP systems to meet local needs. If this is done globally, there is the potential to save thousands of lives a day with this technology.

Acknowledgments: This work was supported by Fulbright Finland, the American Society of Heating, Refrigeration, and Air Conditioning Engineers Graduate Research Fellowship and the University of Colorado at Boulder Technology Transfer Office Proof of Concept Grant. This article represents the views of the authors, and does not necessarily represent the views of Fulbright Finland, the Global Catastrophic Risk Institute or the Alliance to Feed the Earth in Disasters. The authors would also like to thank Michael Brandemuehla, John Zhai, Ray Radebaugh, Moncef Krarti, Jill Stone and Andrew Bour for helpful discussions.

Author Contributions: Joshua M. Pearce conceived and designed the open design analysis; David C. Denkenberger coded and conducted the simulations; Joshua M. Pearce and David C. Denkenberger analyzed the data and wrote the paper.

Conflicts of Interest: The authors declare no conflict of interest. The funding sponsors had no role in the design of the study; in the collection, analyses, or interpretation of data; in the writing of the manuscript, nor in the decision to publish the results.

Appendix A

Table A1. Nomenclature.

Symbol	Units	Explanation
A	m^2	Heat transfer area
C	-	Heat capacity rate ratio
C_c	W/K	Cold heat capacity rate
C_h	W/K	Hot heat capacity rate
C_p	J/(kgK)	Specific heat at constant pressure
E_{fuel}	$	Expenditure on fuel
E_{HX}	$	Expenditure on heat exchanger
$E_{n\text{-}d}$	-	Non-dimensional expenditure
h	$W/(m^2K)$	Heat transfer coefficient
H	hours/year	Utilization of the heat exchanger
HDPE	-	High density polyethylene
HX	-	Heat exchanger
k	W/(mK)	Thermal conductivity
k_1	$\$/m^2$	Price per heat transfer area, constant for optimization
k_2	$1/m^2$	Inverse of area required for one NTU, constant for optimization
k_3	$	Fuel expenditure for zero effectiveness for non-essential heat exchanger case, or unit effectiveness for essential, constant for optimization
LDPE	-	Low density polyethylene
LLDPE	-	Linear low density polyethylene
$\dot{m}$	kg/s	Mass flow rate
NTU	-	Number of transfer units
Nu	-	Nusselt number
P_{fuel}	$/GJ	Price of fuel
P_{HT}	$/(W/K)	Price per heat transfer ability
P_{NTU}	$	Price per NTU
P_V	$\$/m^3$	Price of heat exchanger material per volume
PP	-	Polypropylene
PS	-	Polystyrene
$\dot{q}$	W	Heat transfer rate
r	-	Interest rate
t	m	Wall thickness
T	°C	Temperature
U	$W/(m^2K)$	Overall heat transfer coefficient
Greek		
ΔT_f	K	Temperature change of one of the fluids
ΔT_i	K	Logarithmic mean temperature difference between the hot and cold fluid inside the heat exchanger
ΔT_t	K	Total temperature difference for the heat exchanger
η	-	Effectiveness
Subscripts		
c	-	Cold
e	-	Essential heat exchanger case
h	-	Hot
HT	-	Heat transfer
i	-	In
max	-	Maximum
$n\text{-}e$	-	Non-essential heat exchanger case
o	-	Out
opt	-	Optimum
t	-	Total
w	-	Wall

References

1. World Health Organization. *Monitoring Health for the SDGs: Sustainable Development Goals*; World Health Statistics; World Health Organization: Geneva, Switzerland, 2017; ISBN 978-92-4-156548-6.
2. World Health Organization. *Preventing Diarrhoea through Better Water, Sanitaiton and Hygiene: Exposures and Impacts in Low- and Middle-Income Countries*; World Health Organization: Geneva, Switzerland, 2014; ISBN 978-92-4-156482-3.
3. Prüss-Üstün, A.; Wolf, J.; Corvalán, C.; Bos, R.; Neira, M. *Preventing Disease through Healthy Environments: A Global Assessment of the Burden of Disease from Environmental Risks*, 2nd ed.; World Health Organization: Geneva, Switzerland, 2016; ISBN 978-92-4-156519-6.
4. WHO/UNICEF Joint Water Supply and Sanitation Monitoring Programme. *Progress on Sanitation and Drinking Water*; World Health Organization; UNICEF: Geneve, Switzerland, 2015; ISBN 978-92-4-150914-5.
5. Hutton, G.; Varughese, M. *The Costs of Meeting the 2030 Sustainable Development Goal Targets on Drinking Water, Sanitation, and Hygiene*; The World Bank: Washington, DC, USA, 2016.
6. Hardoon, D. *Wealth: Having it All and Wanting More*; Policy & Practice; Oxfam International: Oxford, UK, 2015.
7. Blanco, J.; Malato, S.; Fernández-Ibañez, P.; Alarcón, D.; Gernjak, W.; Maldonado, M.I. Review of feasible solar energy applications to water processes. *Renew. Sustain. Energy Rev.* **2009**, *13*, 1437–1445. [CrossRef]
8. Khattab, N.M.; Soliman, H.; Metias, M.; El-Seesy, I.; Mettawee, E.; El-Shenawy, E.; Hassan, M. Implementation of Solar Technologies in the Development of Rural, Remote and Sub urban Communities. *Int. J. Therm. Environ. Eng.* **2010**, *3*, 59–66. [CrossRef]
9. Kaushal, A. Varun Solar stills: A review. *Renew. Sustain. Energy Rev.* **2010**, *14*, 446–453. [CrossRef]
10. Velmurugan, V.; Srithar, K. Performance analysis of solar stills based on various factors affecting the productivity—A review. *Renew. Sustain. Energy Rev.* **2011**, *15*, 1294–1304. [CrossRef]
11. Arunkumar, T.; Velraj, R.; Denkenberger, D.C.; Sathyamurthy, R.; Kumar, K.V.; Ahsan, A. Productivity enhancements of compound parabolic concentrator tubular solar stills. *Renew. Energy* **2016**, *88*, 391–400. [CrossRef]
12. Arunkumar, T.; Denkenberger, D.; Ahsan, A.; Jayaprakash, R. The augmentation of distillate yield by using concentrator coupled solar still with phase change material. *Desalination* **2013**, *314*, 189–192. [CrossRef]
13. Arunkumar, T.; Jayaprakash, R.; Denkenberger, D.; Ahsan, A.; Okundamiya, M.; Tanaka, H.; Aybar, H. An experimental study on a hemispherical solar still. *Desalination* **2012**, *286*, 342–348. [CrossRef]
14. Kabeel, A.; Arunkumar, T.; Denkenberger, D.; Sathyamurthy, R. Performance enhancement of solar still through efficient heat exchange mechanism—A review. *Appl. Therm. Eng.* **2017**, *114*, 815–836. [CrossRef]
15. Suneesh, P.; Paul, J.; Jayaprakash, R.; Kumar, S.; Denkenberger, D. Augmentation of distillate yield in "V"-type inclined wick solar still with cotton gauze cooling under regenerative effect. *Cogent Eng.* **2016**, *3*, 1202476. [CrossRef]
16. McGuigan, K.G.; Conroy, R.M.; Mosler, H.-J.; du Preez, M.; Ubomba-Jaswa, E.; Fernandez-Ibañez, P. Solar water disinfection (SODIS): A review from bench-top to roof-top. *J. Hazard. Mater.* **2012**, *235–236*, 29–46. [CrossRef] [PubMed]
17. Dawney, B.; Pearce, J.M. Optimizing the solar water disinfection (SODIS) method by decreasing turbidity with NaCl. *J. Water Sanitat. Hyg. Dev.* **2012**, *2*, 87–94. [CrossRef]
18. Byrne, J.A.; Fernandez-Ibañez, P.A.; Dunlop, P.S.M.; Alrousan, D.M.A.; Hamilton, J.W.J. Photocatalytic Enhancement for Solar Disinfection of Water: A Review. *Int. J. Photoenergy* **2011**, 798051. [CrossRef]
19. Oates, P.M.; Shanahan, P.; Polz, M.F. Solar disinfection (SODIS): Simulation of solar radiation for global assessment and application for point-of-use water treatment in Haiti. *Water Res.* **2003**, *37*, 47–54. [CrossRef]
20. Dawney, B.; Cheng, C.; Winkler, R.; Pearce, J.M. Evaluating the geographic viability of the solar water disinfection (SODIS) method by decreasing turbidity with NaCl: A case study of South Sudan. *Appl. Clay Sci.* **2014**, *99*, 194–200. [CrossRef]
21. Pearce, J.M.; & Denkenberger, D.C. Numerical simulation of the direct application of compound parabolic concentrators to a single effect basin solar still. In Proceedings of the 2006 International Conference of Solar Cooking and Food Processing, Granada, Spain, 12–16 July 2006; Volume 18.

22. Denkenberger, D.C.; Pearce, J.M. Compound parabolic concentrators for solar water heat pasteurization: Numerical simulation. In Proceedings of the 2006 International Conference of Solar Cooking and Food Processing, Granada, Spain, 12–16 July 2006; Volume 18.
23. Burch, J.D.; Thomas, K.E. Water disinfection for developing countries and potential for solar thermal pasteurization. *Solar Energy* **1998**, *64*, 87–97. [CrossRef]
24. Burch, J.; Thomas, K.E. *An Overview of Water Disinfection in Developing Countries and the Potential for Solar Thermal Water Pasteurization*; National Renewable Energy Lab.: Golden, CO, USA, 1998.
25. Safapour, N.; Metcalf, R.H. Enhancement of Solar Water Pasteurization with Reflectors. *Appl. Environ. Microbiol.* **1999**, *65*, 859–861. [PubMed]
26. Onyango, E.A.; Thoruwa, T.F.N.; Maingi, S.M.; Njagi, E.M. Performance of a 2-element plane reflector augmented galvanised pipe flat plate collector for solar water pasteurisation. *J. Food Technol.* **2009**, *7*, 12–19.
27. Duff, W.S.; Hodgson, D.A. A simple high efficiency solar water purification system. *Solar Energy* **2005**, *79*, 25–32. [CrossRef]
28. Bigoni, R.; Kötzsch, S.; Sorlini, S.; Egli, T. Solar water disinfection by a Parabolic Trough Concentrator (PTC): Flow-cytometric analysis of bacterial inactivation. *J. Clean. Prod.* **2014**, *67*, 62–71. [CrossRef]
29. Dayem, A.M.A.; El-Ghetany, H.H.; El-Taweel, G.E.; Kamel, M.M. Thermal performance and biological evaluation of solar water disinfection systems using parabolic trough collectors. *Desalin. Water Treat.* **2011**, *36*, 119–128. [CrossRef]
30. Abraham, J.P.; Plourde, B.D.; Minkowycz, W.J. Continuous flow solar thermal pasteurization of drinking water: Methods, devices, microbiology, and analysis. *Renew. Energy* **2015**, *81*, 795–803. [CrossRef]
31. Amsberry, A.; Tyler, C.; Steinhauff, W.; Pommerenck, J.; Yokochi, A.T.F. Simple Continuous-Flow Device for Combined Solar Thermal Pasteurization and Solar Disinfection for Water Sterilization. *J. Humanit. Eng.* **2015**, *3*, 1–7.
32. Carielo da Silva, G.; Tiba, C.; Calazans, G.M.T. Solar pasteurizer for the microbiological decontamination of water. *Renew. Energy* **2016**, *87*, 711–719. [CrossRef]
33. Carielo, G.; Calazans, G.; Lima, G.; Tiba, C. Solar water pasteurizer: Productivity and treatment efficiency in microbial decontamination. *Renew. Energy* **2017**, *105*, 257–269. [CrossRef]
34. Saitoh, T.S.; El-Ghetany, H.H. Solar water-sterilization system with thermally-controlled flow. *Appl. Energy* **1999**, *64*, 387–399. [CrossRef]
35. Konersmann, L.; Frank, E. *Solar Water Disinfection: Field Test Results and Implementation Concepts*; International Solar Energy Society: Freiburg im Breisgau, Germany, 2011; pp. 1–11.
36. Pearce, J.M. The case for open source appropriate technology. *Environ. Dev. Sustain.* **2012**, *14*, 425–431. [CrossRef]
37. Buitenhuis, J.; Pearce, J.M. Open design-based strategies to enhance appropriate technology development. In Proceedings of the 14th Annual National Collegiate Inventors and Innovators Alliance Conference, San Francisco, CA, USA, 25–27 March 2010; pp. 1–12.
38. Oberloier, S.; Pearce, J.M. General Design Procedure for Free and Open-Source Hardware for Scientific Equipment. *Designs* **2017**, *2*, 2. [CrossRef]
39. Pearce, J.M.; Blair, C.M.; Laciak, K.J.; Andrews, R.; Nosrat, A.; Zelenika-Zovko, I. 3-D Printing of Open Source Appropriate Technologies for Self-Directed Sustainable Development. *J. Sustain. Dev.* **2010**, *3*, 17. [CrossRef]
40. King, D.L.; Babasola, A.; Rozario, J.; Pearce, J.M. Mobile Open-Source Solar-Powered 3-D Printers for Distributed Manufacturing in Off-Grid Communities. *Chall. Sustain.* **2014**, *2*, 18–27. [CrossRef]
41. Gwamuri, J.; Franco, D.; Khan, K.Y.; Gauchia, L.; Pearce, J.M. High-Efficiency Solar-Powered 3-D Printers for Sustainable Development. *Machines* **2016**, *4*, 3. [CrossRef]
42. Andreatta, D.; Yegian, D.; Connelly, L.; Metcalf, R. Recent advances in devices for the heat pasteurization of drinking water in the developing world. In *Proceedings of the Intersociety Energy Conversion Engineering Conference, 1994*; American Institute of Aeronautics and Astronautics: Reston, VA, USA, 1994; p. 1741. [CrossRef]
43. Zaheed, L.; Jachuck, R.J.J. Review of polymer compact heat exchangers, with special emphasis on a polymer film unit. *Appl. Ther. Eng.* **2004**, *24*, 2323–2358. [CrossRef]

44. Ashman, S.; Kandlikar, S.G. A Review of Manufacturing Processes for Microchannel Heat Exchanger Fabrication. In Proceedings of the ASME 4th International Conference on Nanochannels, Microchannels, and Minichannels, Limerick, Ireland, 19–21 June 2006; pp. 855–860. [CrossRef]
45. Denkenberger, D.C.; Brandemuehl, M.J.; Pearce, J.M.; Zhai, J. Expanded microchannel heat exchanger: Design, fabrication, and preliminary experimental test. *Proc. Inst. Mech. Eng. A* **2012**, *226*, 532–544. [CrossRef]
46. Garst, S.; Schuenemann, M.; Solomon, M.; Atkin, M.; Harvey, E. Fabrication of multilayered microfluidic 3D polymer packages. In Proceedings of the ECTC '05 Electronic Components and Technology, Lake Buena Vista, FL, USA, 31 May–4 June 2005; Volume 1, pp. 603–610.
47. Bachmann, F.G.; Russek, U.A. Laser welding of polymers using high-power diode lasers. In *Proceedings of the Photon Processing in Microelectronics and Photonics*; International Society for Optics and Photonics: San Jose, CA, USA, 18 June 2002; Volume 4637, pp. 505–519.
48. Pearce, J.M. *Open-Source Lab: How to Build Your Own Hardware and Reduce Research Costs*; Elsevier: New York, NY, USA, 2013; ISBN 978-0-12-410486-0.
49. Laureto, J.J.; Dessiatoun, S.V.; Ohadi, M.M.; Pearce, J.M. Open Source Laser Polymer Welding System: Design and Characterization of Linear Low-Density Polyethylene Multilayer Welds. *Machines* **2016**, *4*, 14. [CrossRef]
50. Arie, M.A.; Shooshtari, A.H.; Tiwari, R.; Dessiatoun, S.V.; Ohadi, M.M.; Pearce, J.M. Experimental characterization of heat transfer in an additively manufactured polymer heat exchanger. *Appl. Ther. Eng.* **2017**, *113*, 575–584. [CrossRef]
51. Denkenberger, D.; Parisi, M.; Pearce, J.M. Towards Low-Cost Microchannel Heat Exchangers: Vehicle Heat Recovery Ventilator Prototype. In Proceedings of the 10th International Conference on Heat Transfer, Fluid Mechanics and Thermodynamics (HEFAT), Orlando, FL, USA, 14–16 July 2014.
52. Borbely, A.-M.; Kreider, J.F. *Distributed Generation*; CRC Press: New York, NY, USA, 2001.
53. Smith, E.M. *Advances in Thermal Design of Heat Exchangers: A numerical approach: Direct-Sizing, Step-Wise Rating, and Transients*; John Wiley & Sons: Hoboken, NJ, USA, 2005.
54. Grandinetti, J. Safe Water Systems. Personal communication, 2010.
55. Grafman, L. To Catch the Rain. 2018. Available online: http://www.tocatchtherain.org/ (accessed on 23 March 2018).
56. Meera, V.; Ahammed, M.M. Water quality of rooftop rainwater harvesting systems: A review. *J. Water Supply Res. Technol. AQUA* **2006**, *55*, 257–268.
57. Reyneke, B.; Cloete, T.E.; Khan, S.; Khan, W. Rainwater harvesting solar pasteurization treatment systems for the provision of an alternative water source in peri-urban informal settlements. *Environ. Sci. Water Res. Technol.* **2018**, *4*, 291–302. [CrossRef]
58. Canessa, E.; Fonda, C.; Zennaro, M. *Low–Cost 3D Printing for Science, Education and Sustainable Development*; ICTP—The Abdus Salam International Centre for Theoretical Physics: Trieste, Italy, 2013; ISBN 92-95003-48-9.
59. Birtchnell, T.; Hoyle, W. *3D Printing for Development in the Global South: The 3D4D Challenge*; Springer: Berlin, Germany, 2014; ISBN 978-1-137-36566-8.
60. James, E.; Gilman, D. Shrinking the Supply Chain: Hyperlocal Manufacturing and 3D Printing in Humanitarian Response. In *OCHA Policy and Studies Series*; OCHA: New York, NY, USA, 2015; Volume 14.
61. De la Torre, N.; Espinosa, M.M.; Domínguez, M. Rapid Prototyping in Humanitarian Aid to Manufacture Last Mile Vehicles Spare Parts: An Implementation Plan. *Hum. Factors Ergon. Manuf. Serv. Ind.* **2016**, *26*, 533–540. [CrossRef]
62. James, E.; James, L. 3D Printing Humanitarian Supplies in the Field. *Humanit. Exch.* **2016**, *66*, 43–45.
63. Loy, J.; Tatham, P.; Healey, R.; Tapper, C.L. 3D Printing Meets Humanitarian Design Research: Creative Technologies in Remote Regions. *Creat. Technol. Multidiscip. Appl.* **2016**, 54–75. [CrossRef]
64. McBride, A. 3D Printing Takes Emergency Response to another Level. Policy and Practice Blog, 2014. Available online: https://policy-practice.oxfam.org.uk/blog/2014/05/3d-printing-takes-emergency-response-to-another-level (accessed on 4 February 2018).
65. Ott, D. Can Digital Fabrication Revolutionise Humanitarian Action? ICRC Blog, 2016. Available online: http://blogs.icrc.org/gphi2/2016/02/22/can-digital-fabrication-revolutionize-humanitarian-action/ (accessed on 4 February 2018).

66. Scott, C. ICRC Enable Makeathon Endeavors to Help People with Disabilities in Remote Areas through 3D Printing and Other Technologies. 3D Print, 2015. Available online: https://3dprint.com/tag/icrc/ (accessed on 4 February 2018).
67. Saripalle, S.; Maker, H.; Bush, A.; Lundman, N. 3D Printing for Disaster Preparedness: Making Life-Saving Supplies on-Site, on-Demand, on-Time. In Proceedings of the IEEE Global Humanitarian Technology Conference, Seattle, WA, USA, 13–16 October 2016; pp. 205–208.
68. Savonen, B.L.; Mahan, T.J.; Curtis, M.W.; Schreier, J.W.; Gershenson, J.K.; Pearce, J.M. Development of a Resilient 3-D Printer for Humanitarian Crisis Response. *Technologies* **2018**, *6*, 30. [CrossRef]
69. Thryft, A.R. This Startup Wants Industrial 3D Printing to be Affordable in the Developing World. Available online: https://www.designnews.com/content/startup-wants-industrial-3D-printing-be-affordable-developing-world/119436841439281 (accessed on 13 March 2018).
70. ESD Ultem 3D Printing Filament, 3DXTech. 2018. Available online: https://www.3dxtech.com/esd-ultem-3d-printing-filament/ (accessed on 23 March 2018).
71. Tyson, E. Want to Use ABS in Hot Sun? We Compare ABS vs. ASA Filaments, Rigid Ink. 2016. Available online: https://rigid.ink/blogs/news/175845063-the-difference-between-abs-and-asa (accessed on 23 March 2018).
72. Doalman, J.D.B. The mystery of electronic water treatment unveiled. *Ind. Technol. News* **2005**, *25*.
73. Shah, R.K.; Subbarao, E.C.; Mashelkar, R.A. *Heat Transfer Equipment Design*; CRC Press: Boca Raton, FL, USA, 1988; ISBN 978-0-89116-729-7.
74. Goddard, J.B. *Abrasion Resistance of Piping Systems*; ADS Technical Note 2.116; Advanced Drainage Syst.: Hilliard, OH, USA, 1994.
75. Bongaarts, J. Can family planning programs reduce high desired family size in sub-Saharan Africa? *Int. Perspect. Sex. Reprod. Health* **2011**, *37*, 209–216. [CrossRef] [PubMed]
76. National Research Council. *Water and Sustainable Development: Opportunities for the Chemical Sciences: A Workshop Report to the Chemical Sciences Roundtable*; National Academies Press: Washington, DC, USA, 2004.
77. Pearce, J.M. Applications of open source 3-D printing on small farms. *Org. Farming* **2015**, *1*, 19–35. [CrossRef]
78. Baechler, C.; DeVuono, M.; Pearce, J.M. Distributed recycling of waste polymer into RepRap feedstock. *Rapid Prototyp. J.* **2013**, *19*, 118–125. [CrossRef]
79. Cruz Sanchez, F.A.; Lanza, S.; Boudaoud, H.; Hoppe, S.; Camargo, M. Polymer Recycling and Additive Manufacturing in an Open Source context: Optimization of processes and methods. In Proceedings of the Annual International Solid Freeform Fabrication Symposium (ISSF), Austin, TX, USA, 10–12 August 2015; pp. 1591–1600.
80. Cruz Sanchez, F.A.; Boudaoud, H.; Hoppe, S.; Camargo, M. Polymer recycling in an open-source additive manufacturing context: Mechanical issues. *Addit. Manuf.* **2017**, *17*, 87–105. [CrossRef]
81. Anderson, I. Mechanical Properties of Specimens 3D Printed with Virgin and Recycled Polylactic Acid. *3D Print. Addit. Manuf.* **2017**, *4*, 110–115. [CrossRef]
82. Pakkanen, J.; Manfredi, D.; Minetola, P.; Iuliano, L. About the Use of Recycled or Biodegradable Filaments for Sustainability of 3D Printing. In *Sustainable Design and Manufacturing*; Smart Innovation, Systems and Technologies; Springer: Cham, Switzerland, 2017; pp. 776–785.
83. Chong, S.; Pan, G.-T.; Khalid, M.; Yang, T.C.-K.; Hung, S.-T.; Huang, C.-M. Physical Characterization and Pre-assessment of Recycled High-Density Polyethylene as 3D Printing Material. *J. Polym. Environ.* **2017**, *25*, 136–145. [CrossRef]
84. Mohammed, M.I.; Mohan, M.; Das, A.; Johnson, M.D.; Badwal, P.S.; McLean, D.; Gibson, I. A low carbon footprint approach to the reconstitution of plastics into 3D-printer filament for enhanced waste reduction. *KnE Eng.* **2017**, *2*, 234–241. [CrossRef]
85. Mohammed, M.I.; Das, A.; Gomez-Kervin, E.; Wilson, D.; Gibson, I. EcoPrinting: Investigating the use of 100% recycled Acrylonitrile Butadiene Styrene (ABS) for Additive Manufacturing. Solid Freeform Fabrication 2017. In Proceedings of the 28th Annual International Solid Freeform Fabrication Symposium, Austin, TX, USA, 13–15 August 2018; Available online: http://sffsymposium.engr.utexas.edu/sites/default/files/2017/Manuscripts/EcoprintingInvestigatingtheUseof100Recycle.pdf (accessed on 3 March 2018).
86. Zhong, S.; Pearce, J.M. Tightening the loop on the circular economy: Coupled distributed recycling and manufacturing with recyclebot and RepRap 3-D printing. *Resour. Conserv. Recycl.* **2018**, *128*, 48–58. [CrossRef]

87. Pringle, A.M.; Rudnicki, M.; Pearce, J. Wood Furniture Waste-Based Recycled 3-D Printing Filament. *For. Prod. J.* **2018**. [CrossRef]
88. Tian, X.; Liu, T.; Wang, Q.; Dilmurat, A.; Li, D.; Ziegmann, G. Recycling and remanufacturing of 3D printed continuous carbon fiber reinforced PLA composites. *J. Clean. Prod.* **2017**, *142*, 1609–1618. [CrossRef]
89. Appropedia. 2018. Available online: http://www.appropedia.org/ (accessed on 23 March 2018).